Quantum-Chemical Studies to Approach the Antioxidant Mechanism of Nonphenolic Hydrazone Schiff Base Analogs: Synthesis, Molecular Structure, Hirshfeld and Density Functional Theory Analyses

Mohammad Sayed Alam and Dong-Ung Lee*

Division of Bioscience, Dongguk University, Gyeongju 780-714, Republic of Korea.
**E-mail: dulee@dongguk.ac.kr*
Received October 10, 2014, Accepted December 3, 2014, Published online January 30, 2015

In the present study, five nonphenolic (*E*)-*N*′-benzylidenebenzohydrazides including three new compounds were synthesized and evaluated for their free radical scavenging activities using 2,2-diphenyl-1-picrylhydrazyl (DPPH). X-Ray analysis of a single crystal of (*E*)-*N*′-(4-chlorobenzylidene)benzohydrazide (**3c**) revealed a triclinic, space group P-1 structure with a *trans* configuration around the azomethine (—C2═N2—) double bond. The three-dimensional Hirshfeld surfaces and the related two-dimensional fingerprint plots were also drawn to study the plausible intermolecular interactions. Density functional calculations of structures, electronic densities, frontier molecular orbitals modeling, and Mulliken charge analysis of all compounds were performed at the B3LYP/6-311G level of theory. Theoretical vibrational frequencies were predicted and compared with experimental values, and results supported the validity of optimized geometry of noncrystalline compounds. All synthesized compounds showed significant DPPH radical scavenging activity, although compound **3d** exhibited greatest antioxidant activity with an IC_{50} value of 11 μM. The results of DFT analysis were used to explain the proposed antioxidant mechanism of (*E*)-*N*′-benzylidenebenzohydrazide analogs. This analysis revealed that protons attached to N, O, and C atoms possessing high negative charge are involved in the production of free radicals that scavenge DPPH. Moreover, the antioxidant activities of (*E*)-*N*′-benzylidenebenzohydrazide analogs correlated well with HOMO–LUMO energy difference of molecules.

Keywords: Benzylidenebenzohydrazides, Crystal structure, Antioxidant activity, DFT-B3LYP calculation

Introduction

Hydrazide–hydrazone Schiff bases are the class of compounds with an azomethine (—N═CH—) active pharmacophore and have significant biological activities. This class of compounds has been reported to exhibit diverse biological activities, such as, antimicrobial,[1] antioxidant,[2] anticancer,[3] antitubercular,[4] anticonvulsant,[5] anti-inflammatory,[6] antifungal,[7] antiviral,[8] and antibacterial[9] activities. Recently, Ayman et al.[10] described the pro-angiogenic and anticancer activities of Schiff bases of *N*-valproyl-4-aminobenzoyl hydrazide. Hydrazone Schiff bases are also used as ligands to form variety of complexes with transition and inner transition metals that have wide-ranging biological activities.[11–13] Not surprisingly these biological activities and applications of hydrazone Schiff bases have attracted the attention of many researchers.

Oxidative stress generates various reactive oxygen species (ROS) that can cause DNA damage leading to deleterious biological consequences, which include genetic mutation, carcinogenesis, and cell death.[14,15] Free radicals have also been reported to play important roles during aging, cardiovascular diseases, rheumatoid arthritis, and other pathologies. Antioxidants can neutralize free radicals and provide protection against diseases caused by ROS. Therefore, much research effort is being expended to identify potential antioxidants that are capable of affording protection against potentially fatal diseases caused by oxidative DNA damage. The antioxidant mechanism of phenolics are well documented and involve processes, such as, hydrogen atom transfer (HAT), proton-coupled electron transfer (PCET), electron transfer–proton transfer (ET–PT), sequential proton loss single electron transfer (SPLET), sequential electron–proton transfer (SEPT), and adduct formation.[16–20] For this reason, it is also important to determine mechanisms responsible for the activities of nonphenolic antioxidants with the aims of improving potency and discovering new antioxidant agents to fight against the fatal diseases caused by free radicals. In the present study, we report the antioxidant mechanism of nonphenolic (*E*)-*N*′-benzylidenebenzohydrazide analogs together with the synthesis, crystal structure, and Hirshfeld analyses. The structural geometries, electronic densities, and frontier molecular orbitals (FMOs) modeling of the compounds were studied at the B3LYP/6-311G level of theory to explain the antioxidant mechanism of nonphenolic (*E*)-*N*′-benzylidenebenzohydrazide analogs.

Experimental

General. All commercially available reagents and solvents were purchased from Sigma-Aldrich (St. Louis, MO, USA)

and used without further purification. The melting points (uncorrected) of synthesized compounds were determined using a Stuart SMP3 apparatus (Bibby Sci. Ltd., Staffordshire, UK). FT-IR spectra were obtained using a Bruker Tensor 37 spectrometer and KBr discs. NMR spectra were recorded using a Bruker 400 MHz spectrometer (Billerica, MA, USA) in dimethyl sulfoxide. Mass spectra were acquired using a Jeol JMS700 high-resolution mass spectrometer (Tokyo, Japan) at the Korea Basic Science Center (Daegu, Korea). Elemental analyses (C, H, and N) were performed on a PerkinElmer 2400 II CHN elemental analyzer (PerkinElmer, Waltham, MA, USA).

General Procedure for the Preparation of (*E*)-*N*′-Benzylidenebenzohydrazide Analog (3a–e). Compounds **3a–e** were prepared as described in a previous report.[2] Briefly, to a stirred solution of benzohydrazide (**2**, 10 mM) in 30 mL ethanol, a suitably substituted benzaldehyde (10 mM) in 20 mL ethanol was added slowly and refluxed for 1.5–2.5 h. On reaction completion (progress was monitored by TLC), reaction mixtures were cooled to room temperature and filtered to give solid crude products, which were then crystallized from ethanol to provide the pure compounds. The IR, ^{1}H NMR, mass spectrometry, and elemental analysis data of compounds **3a–e** are provided as supporting information.

Crystal Structure Determination. The solvent loss technique was used to grow white plate-shaped crystals of **3c**. A single crystal of suitable size (0.23 mm × 0.11 mm× 0.05 mm) was chosen for the X-ray diffraction study. Data were collected at a temperature of 193(2) K from a Bruker *SMART* CCD area detector diffractometer[21] operating with graphite monochromated radiation Mo$K\alpha$ ($\lambda = 0.71073$ Å). A total of 22,530 reflections were collected, of which 3007 ($-7 \le h \le 7$, $-10 \le k \le 10$, $-19 \le l \le 19$) were treated as observed. The structure was solved by direct methods using SHELXTL.[22] Full-matrix least-squares refinement using SHELXTL with isotropic displacement parameters for all nonhydrogen atoms converged the residual to $R_1 = 0.1342$. Subsequent refinements[23] were carried out using anisotropic thermal parameters for nonhydrogen atoms. Hydrogen atoms were fixed at chemically acceptable positions and were allowed to ride on parent atoms at a C—H distance of 0.9500 Å. The final refinement converged to $R = 0.0442$, $wR = 0.1202$, $w = 1/[\sigma^2(F_o)^2 + (0.0680P)^2 + 0.42P]$, where $R = \Sigma(|F_o| - |F_c||)/\Sigma|F_o|$, F_o = observed structure factor, F_c = calculated structure factor, $P = (F_o^2 + 2F_c^2)/3$, $\sigma = 1.053$, $(\Delta/\sigma)_{max} < 0.001$, $(\Delta\rho)_{max} = 0.347$ and $(\Delta\rho)_{min} = -0.318$ e/Å^3.

2,2-Diphenyl-1-picrylhydrazyl Radical Scavenging Activity. Free radical-scavenging activities of the synthesized compounds were assayed as described by Blois[24] with some modifications using 2,2-diphenyl-1-picrylhydrazyl (DPPH). Briefly, to 0.1 mL samples of compounds **3a–e** at different concentrations in ethanol, 4 mL of 1.5×10^{-5} M DPPH solution was added, thoroughly mixed, and left to stand at room temperature in a dark place for 30 min. Solution absorbances were then measured at 520 nm, and used to calculate DPPH radical scavenging activities (%) using the following equation:

$$\text{DPPH radical-scavenging activity (\%)} = [(\text{Absorbance of the control} - \text{Absorbance of the sample})/\text{Absorbance of the control}) \times 100]$$

Computational Studies. The molecular geometries of the (*E*)-*N*′-benzylidenebenzohydrazide analogs (**3a–e**) were optimized by MM+ molecular modeling and by using semi-empirical molecular orbital AM1 methods.[25] Density functional theory (DFT) calculations with a hybrid functional B3LYP (Becke's three parameter nonlocal exchange functional along with the Lee-Yang-Parr correlation function)[26,27] at basis set 6-311G were then performed using the GAMESS interface in ChemBio3D ultra ver. 14.0 (PerkinElmer). No imaginary frequencies were obtained during vibrational frequency calculations, indicating that all structures were stable. After optimization, Mulliken charge and properties of FMOs of all compounds were analyzed using results calculated at the B3LYP/ 6-311G level. Hirshfeld surfaces and the related two-dimensional (2D) fingerprint plots were calculated using Crystal Explorer 3.1.[28]

Results and Discussion

Synthesis, Crystal Structure, and Hirshfeld Analyses. The synthetic pathway of hydrazone Schiff base analogs (**3a–e**) is shown in Scheme 1. Products were obtained in excellent yields

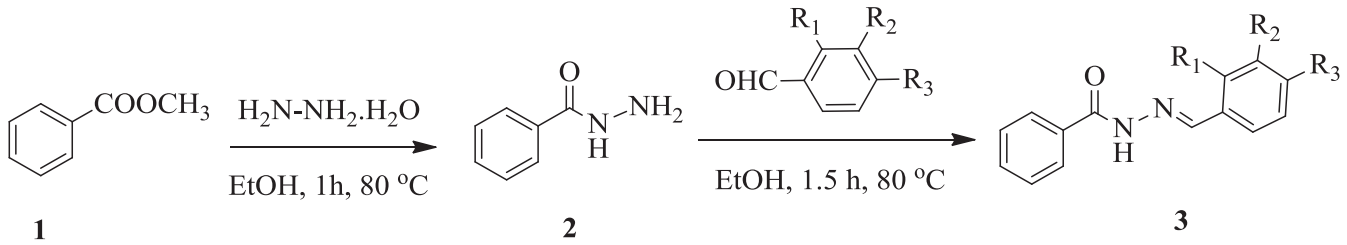

3a. $R_1, R_2 = H, R_3 = H$; **3b.** $R_1 = H, R_2, R_3 = OCH_3$; **3c.** $R_1, R_2 = H, R_3 = Cl$; **3d.** $R_1, R_2 = H, R_3 = N(CH_3)_2$; **3e.** $R_1 = CHO, R_2, R_3 = H$.

Scheme 1. The synthetic pathway of hydrazone Schiff base analogs (**3a–e**).

(81–96%). Compounds **3b**, **3d**, and **3e** are new. The syntheses of compounds **3a** and **3c** have already been reported;[29] however, the crystal structure, Hirshfeld analyses of compound **3c**, as well as DFT studies and antioxidant activity of compounds **3a–e**, have not yet been reported. The structures of the synthesized compounds were elucidated using IR, ^{1}H NMR, mass spectra, and elemental analyses, which are provided as supporting information. The IR spectra of compounds **3a–e** showed an absorption band around the 3174–3437 cm^{-1} region resulting from ─NH─ stretch. The stretching absorption band of >C═O appeared at 1641–1667 cm^{-1}. ^{1}H NMR spectra of compounds **3a–e** showed singlet protons at 8.13–8.70 ppm corresponding to the ─CH═N─ proton and at 11.00–11.94 ppm for the ═N─NH─ proton. Aromatic and other functional group protons appeared in their usual positions. The EI-MS spectra of **3a–e** showed molecular ion peaks with intensities of 22–35%.

Among five compounds (**3a–e**), **3c** was analyzed with X-ray diffractometer system, because only this compound could be crystallized as single white crystals by slow evaporation from ethanol and other compounds were obtained in powder form. The displacement ellipsoid plot of **3c**, at a 50% probability and with the numbering scheme is shown in Figure 1(a). X-Ray diffraction crystal data and refinements are presented in Table 1. Selected bond lengths and angles are listed in Table 2. Detailed atomic coordinates, thermal parameters, and torsion angles are detailed in supplementary materials. Compound **3c** crystallized in the triclinic, space group P-1 with $a = 5.3742(2)$ Å, $b = 7.7205(3)$ Å, $c = 14.9609(6)$ Å, $\alpha = 100.2540(16)°$, $\beta = 92.6700(15)°$, $\gamma = 90.6900(16)°$, $V = 610.04(4)$ Å^3, $Z = 2$, $D_c = 1.408$ Mg/m^3, $F(000) = 268$, $\mu = 0.301$ mm^{-1}, $R = 0.0422$, and $wR = 0.1202$. In **3c**, two phenyl rings were found to be linked by a open-chain carbonyl-hydrazone (─C═N─NH─CO─) system, in which C2, N2, N1, C1, and O1 atoms were almost in the same plane with dihedral angle of −3.3(3)° between O(1)─C(1)─N(1)─N(2) and of −10.5(4)° between C(2)─N(2)─N(1)─C(1). As was expected, **3c** adopts a *trans* configuration about the ─N2═C2─ double bond. Furthermore, the *p*-chlorophenyl ring of **3c** is nearly coplanar with the plane formed by ─C2═N2─ with a dihedral angle of −15.2(3)°. The second

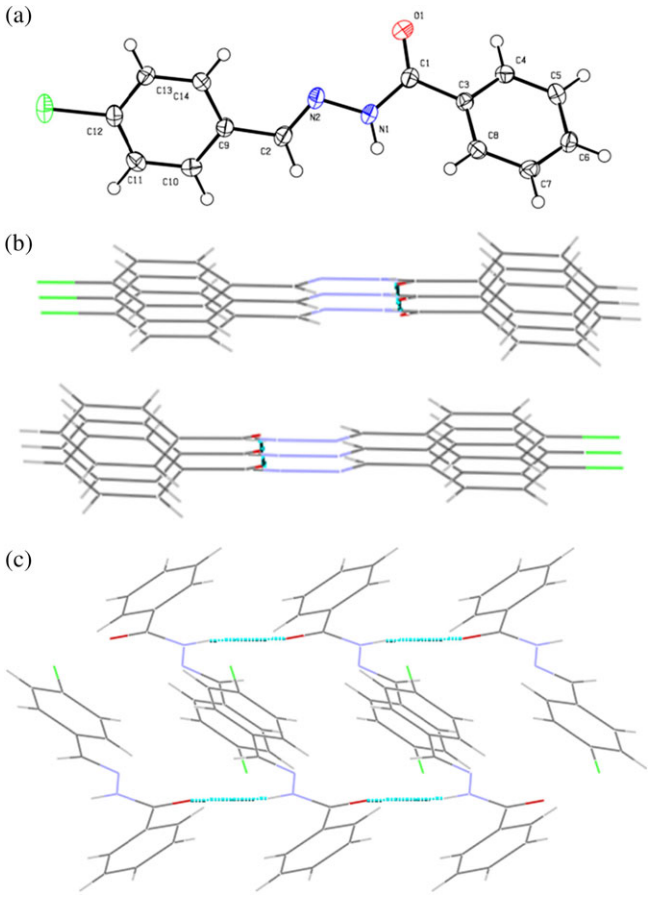

Figure 1. (a) The molecular structure of (*E*)-*N*′-(4-chlorobenzylidene)benzohydrazide (**3c**), showing 50% probability displacement ellipsoids and the atom-numbering scheme. (b, c) Packing arrangements in the crystal structure of **3c** in different views. Blue *dashed lines* indicate hydrogen bonds.

Table 1. Crystal data and structure refinement for (*E*)-*N*′-(4-chlorobenzylidene)benzohydrazide (**3c**).

Empirical formula	$C_{14}H_{11}ClN_2O$	
Formula weight	258.70	
Temperature	193(2) K	
Wavelength	0.71073 Å	
Crystal system	Triclinic	
Space group	P-1	
Unit cell dimensions	$a = 5.3742(2)$ Å	$\alpha = 100.2540(16)°$
	$b = 7.7205(3)$ Å	$\beta = 92.6700(15)°$
	$c = 14.9609(6)$ Å	$\gamma = 90.6900(16)°$
Volume	610.04(4) Å^3	
Z	2	
Density (calculated)	1.408 Mg/m^3	
Absorption coefficient	0.301 mm^{-1}	
F(000)	268	
Crystal size	0.23 × 0.11 × 0.05 mm^3	
Theta range for data collection	2.68–28.34°	
Index ranges	$-7 \le h \le 7$, $-10 \le k \le 10$, $-19 \le l \le 19$	
Reflections collected	22530	
Independent reflections	3007 [R(int) = 0.0421]	
Completeness to theta = 28.34°	98.6%	
Absorption correction	Semi-empirical from equivalents	
Max. and min. transmission	0.9851 and 0.9340	
Refinement method	Full-matrix least-squares on F^2	
Data/restraints/parameters	3758/0/201	
Goodness-of-fit on F^2	1.053	
Final R indices [$I > 2\sigma(I)$]	$R_1 = 0.0422$, $wR_2 = 0.1202$	
R indices (all data)	$R_1 = 0.0534$, $wR_2 = 0.1342$	
Largest diff. peak and hole	0.347 and −0.318 e/Å	
CCDC deposit number	CCDC 1017656	

phenyl ring (C3—C8) of **3c** is significantly rotated out of the plane formed by the remainder of the molecule at an angle of −32.1(2)°. The torsion angle values of N(2)—C(2)—C(9)—C(10) and N(1)—C(1)—C(3)—C(4) were 166.30(16)° and 147.57(16)°, respectively. Figure 1(b) and (c) shows the crystal packing arrangement of **3c** in different views and intermolecular hydrogen bonding interactions. The bond lengths and angles related to H-bonding are summarized in Table 3. Briefly, the H-atom attached to N1 is involved in hydrogen bond formation with the O(1)-atom of another molecule to form a layer. As shown in Figure 2(b), molecules in different layer are juxtaposed. No H-bonds were observed between layers, and thus, crystal formation appears to depend of weak van der Waals forces.

Table 2. Selected bond lengths (Å) and angles (°) as determined by X-ray crystallography for (*E*)-*N*′-(4-chlorobenzylidene) benzohydrazide (**3c**).

Bond lengths (Å)		Bond angles (°)	
C(1)—O(1)	1.223(2)	O(1)—C(1)—N(1)	123.92(15)
C(1)—N(1)	1.359(2)	O(1)—C(1)—C(3)	121.80(15)
C(1)—C(3)	1.502(2)	N(1)—C(1)—C(3)	114.22(14)
N(1)—N(2)	1.3847(18)	C(1)—N(1)—N(2)	120.82(14)
N(1)—H(1)	0.8800	C(1)—N(1)—H(1)	119.6
N(2)—C(2)	1.281(2)	N(2)—N(1)—H(1)	119.6
C(2)—C(9)	1.470(2)	C(2)—N(2)—N(1)	113.27(14)
C(3)—C(4)	1.389(2)	N(2)—C(2)—C(9)	121.39(15)
C(3)—C(8)	1.396(2)	C(4)—C(3)—C(8)	119.50(15)
C(4)—C(5)	1.389(2)	C(4)—C(3)—C(1)	117.31(14)
C(5)—C(6)	1.388(3)	C(8)—C(3)—C(1)	123.18(14)
C(6)—C(7)	1.390(3)	C(5)—C(4)—C(3)	120.53(15)
C(7)—C(8)	1.394(2)	C(6)—C(5)—C(4)	120.02(16)
C(9)—C(14)	1.395(2)	C(5)—C(6)—C(7)	119.80(15)
C(9)—C(10)	1.401(2)	C(6)—C(7)—C(8)	120.28(15)
C(10)—C(11)	1.388(2)	C(7)—C(8)—C(3)	119.85(15)
C(11)—C(12)	1.383(2)	C(14)—C(9)—C(10)	119.05(15)
C(12)—C(13)	1.390(2)	C(14)—C(9)—C(2)	122.82(15)
C(12)—Cl(1)	1.7407(16)	C(10)—C(9)—C(2)	118.11(15)
C(13)—C(14)	1.390(2)	C(11)—C(10)—C(9)	120.62(15)
		C(12)—C(11)—C(10)	119.09(15)
		C(11)—C(12)—C(13)	121.59(15)
		C(11)—C(12)—Cl(1)	119.01(13)
		C(13)—C(12)—Cl(1)	119.40(13)
		C(12)—C(13)—C(14)	118.87(15)
		C(13)—C(14)—C(9)	120.76(15)

Table 3. Hydrogen-bond geometries (Å, °) in (*E*)-*N*′-(4-chlorobenzylidene)benzohydrazide (**3c**)

D—H···A	D—H (Å)	H···A (Å)	D···A (Å)	D—H···A (°)
N(1)—H(1)···O(1)^{i}	0.88	2.33	3.1434(19)	154.2

Symmetry code: (i) $x-1$, y, and z.

Hirshfeld surface analyses[30] are a unique approach to visualize and explore for the individual types of intermolecular interactions within the crystal structure. Hirshfeld surface mapped with d_{norm} using red–white–blue color scheme where it is indicating shorter contacts, vdW contacts and longer contacts, respectively. Fingerprint plots generated based on the d_e and d_i distances where d_e is the distance from the Hirshfeld surface to the nearest atom outside the surface and d_i is the distance from the Hirshfeld surface to the nearest atom inside the surface. Hirshfeld surface analysis and the associated 2D fingerprint plots of **3c** were performed using CrystalExplorer software. The Hirshfeld surfaces of compound **3c** have been mapped over d_{norm} (−0.5 to 1.5 Å) and showing the deep red circular depressions visible in the front and back views of surfaces are indicating hydrogen bonding contacts (Figure 2). The strong interactions between C—H and N—H and carbonyl O atoms can be seen in the Hirshfeld surface as red areas. Some significant π–π interactions are also observed in Figure 2(c), showing red and blue triangles representing the presence of π–π stacking. In the 2D fingerprint plot of **3c** appeared four distinct spikes indicating different interactions can occur between two different molecules in the crystal structure (Figure 3). The visible complementary regions in the fingerprint plots showing one molecule acts as a donor ($d_e > d_i$) and the other as an acceptor ($d_e < d_i$). The C—H···O, C—H···N, C—H···Cl and C—H···C intermolecular interactions appear as one spike each in the 2D fingerprint plots for compound **3c**.

DFT Calculations, Vibrational Frequencies, FMO Energies, and Mulliken Charge Distributions. DFT has received much interest as reliable tool for the quantum-chemical calculations of molecular structures and biological properties of molecules. In the present study, quantum-chemical calculations were carried out using DFT at the B3LYP/6-311G level of theory to determine the properties of FMOs and Mulliken charge distributions to explain the mechanism responsible for the DPPH free-radical scavenging activities of the nonphenolic hydrazone Schiff base analogs (**3a–e**). The optimized geometric parameters of compounds **3a–e** at the B3LYP/6-311G level are provided in Tables S1 and S2 (Supporting information). The calculated bond lengths and angles of compounds **3a–e** were within normal ranges,[31] but showed small deviations from experimental values (Table 2), presumably because theoretical calculations are based on the isolated

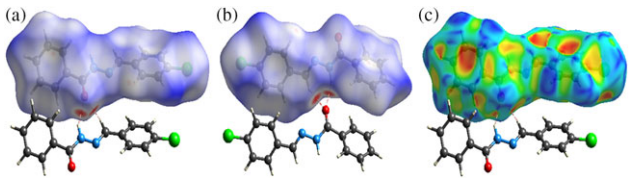

Figure 2. Hirshfeld map with d_{norm} (front view, a and back view, b), where deep red circle indicating hydrogen bonding contacts, and shape index (c), where red (δ^-) and blue (δ^+) surfaces showing π–π stacking, noncovalent attractive force for compound **3c**.

molecules in the gaseous phase whereas experimental results are obtained in the solid state. The theoretical structures of the hydrazone Schiff base analogs (**3a–e**) are shown in Figure 4.

The vibrational frequencies of compounds **3a–e** were predicted using DFT at the B3LYP/6-311G level at a spin multiplicity of one; no imaginary frequencies were obtained, indicating that the structures are in stable form. Some selected experimental and calculated harmonic frequencies for compounds **3a–e** are listed in Table S3. Figure S1 provides a comparison of the experimental and simulated infrared spectra of **3d**, a *N*,*N*′-dimethyl analog of (*E*)-*N*′-benzylidenebenzohydrazide, which demonstrated high antioxidant activity. According to the results presented in Table S3 and Figure S1, predicted vibrational frequencies are in well agreement with the experimental values, indicating the validity of the optimized structure of the synthesized compounds.

FMOs play an important part in predicting molecular reactivity and properties. Single point energies and FMOs were

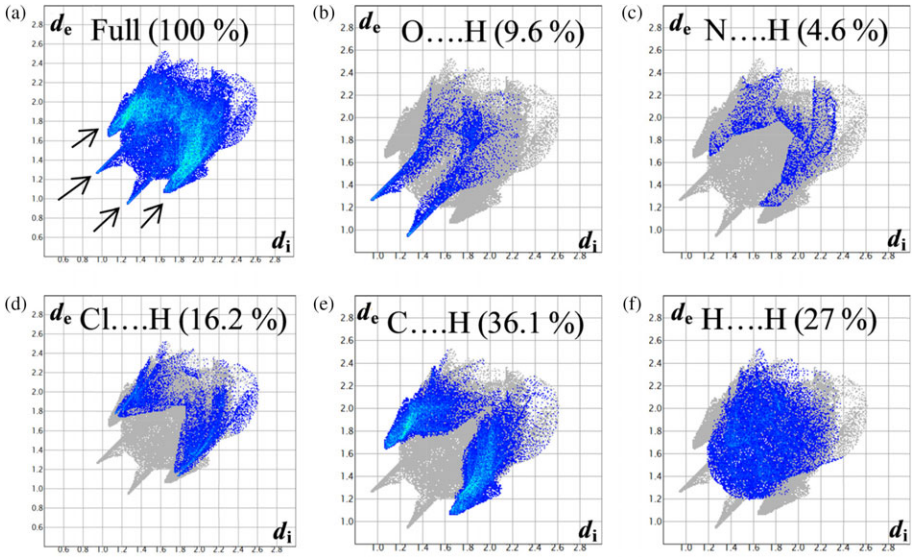

Figure 3. 2D fingerprint plots of compound **3c**, full (a); showing reciprocal contacts and resolved into: O· · ·H (b), N· · ·H (c), Cl· · ·H (d), C· · ·H (e), and H· · ·H (f) showing the percentage of contact contributed to the total Hirshfeld surface area of molecules. Black arrows show spikes for different interactions. d_i is the closest internal distance from a given point on the Hirshfeld surface and d_e is the closest external contacts.

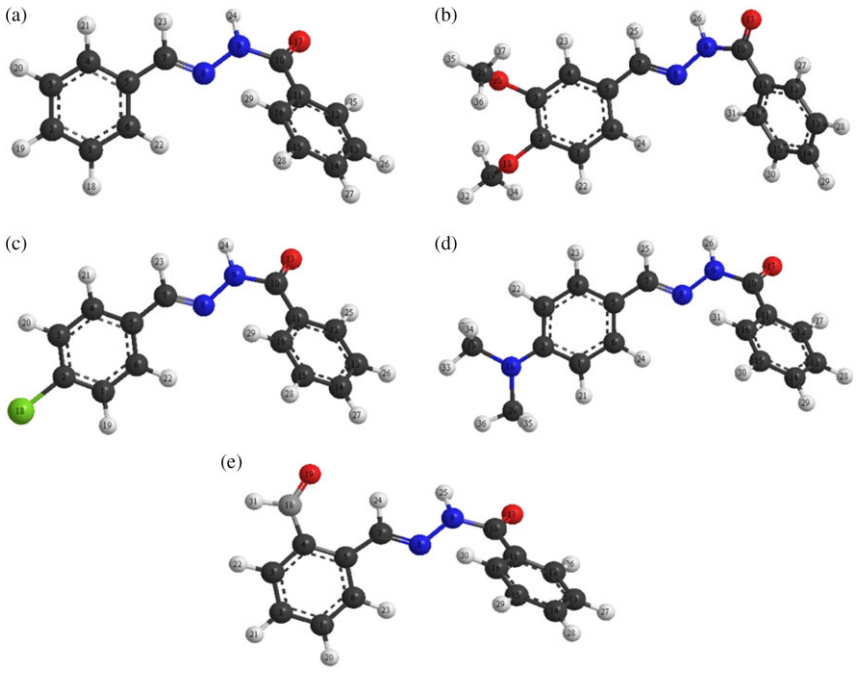

Figure 4. Theoretical geometric structures of **3a** (a), **3b** (b), **3c** (c), **3d** (d), and **3e** (e), and the atom numbering scheme.

determined using quantum chemical calculations. In these calculations, 29 atoms involving 257 basis functions and 59 occupied orbitals for **3a**, 37 atoms involving 321 basis functions and 75 occupied orbitals for **3b**, 29 atoms involving 275 basis functions and 67 occupied orbitals for **3c**, 37 atoms involving 311 basis functions and 71 occupied orbitals for **3d**, and 31 atoms involving 283 basis functions and 66 occupied orbitals for **3e**, were identified. The energy levels of HOMO and LUMO for **3a**, **3b**, **3c**, **3d**, and **3e** are provided in Figure 5. The total energies of **3a** (−724 a.u.), **3b** (−953 a.u.), **3c** (−1184 a.u.), **3d** (−858 a.u.), and **3e** (−838 a.u.), and the energies of HOMO and LUMO including neighboring orbitals were all negative, indicating that all compounds are stable. HOMO and its vicinal orbitals act as nucleophiles, whereas LUMO and its vicinal orbitals act as electrophiles.

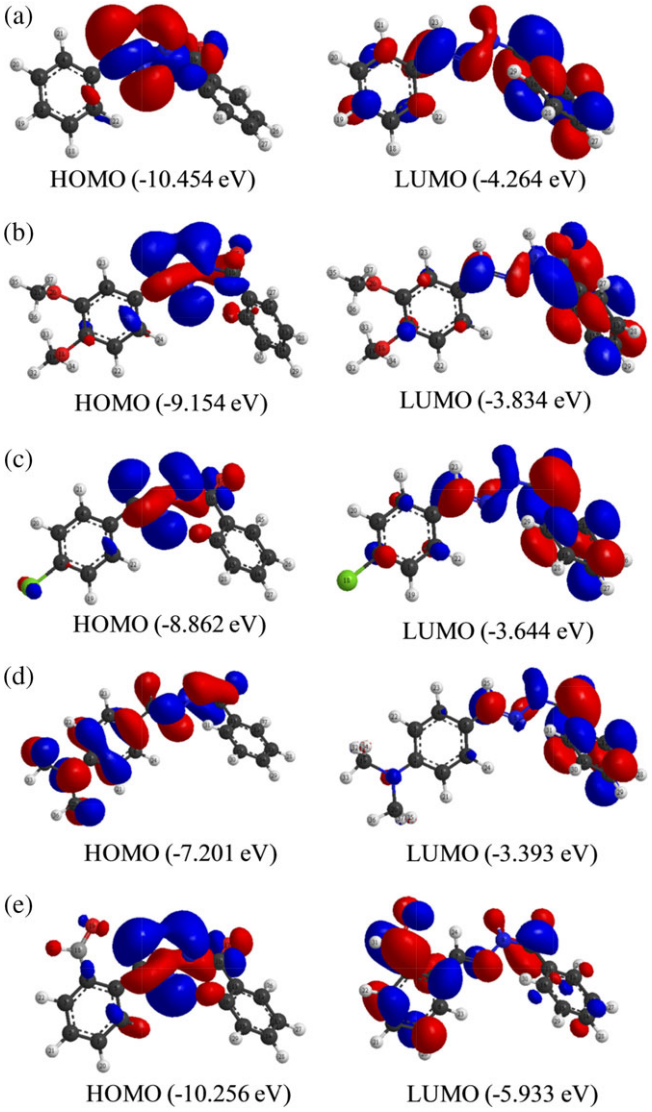

Figure 5. FMOs contour plots (HOMO and LUMO) and the corresponding energies of **3a** (a), **3b** (b), **3c** (c), **3d** (d), and **3e** (e). Different surface colors represent opposite signs of the wave function.

The Mulliken charge distributions of all atoms were calculated based on the optimized geometries of compounds **3a–e**; results are presented in Table 4. According to this analysis, the electro-negativities of bonding atoms play an important role in the distribution of Mulliken charge. As was expected, H and C bonded with O and N atom were all positive, whereas azomethine and imine N atoms, O bonded with C atom, and C bonded with H atom were all negative. So, the hetero atoms N9 and O17 for **3a**, **3c**, and **3d**, N9, O17, O18, and O20 for **3b**, and N9, O17, and O19 for **3e** could act as electron donors and coordinate with metals which is consistent with our previous study.[2]

Antioxidant Activities. Compounds **3a–e** were evaluated for free radical scavenging activities using DPPH. The details of the DPPH antioxidant assay data are provided in Table S4. As presented in Table 5, all compounds exhibited significant DPPH radical scavenging activity. In particular, **3d** showed greatest antioxidant activity with an IC_{50} value of 11.0 μM. The unsubstituted hydrazone Schiff base, that is, (*E*)-*N*′-benzylidenebenzohydrazide (**3a**) showed lowest activity with an IC_{50} value of 360 μM. The 3,4-dimethoxy analog (**3b**, IC_{50} = 164 μM) was ~2.2 times more active than **3a**, and the 4-chloro analog (**3c**, IC_{50} = 264 μM) was ~1.4 times more active. The 4-*N*,*N*-dimethylamino analog (**3d**), which containing a stronger electron-donating group than the other analogs exhibited ~33 times more activity than **3a**, while the 2-formyl analog (**3e**, IC_{50} = 114 μM) containing a stronger electron-withdrawing group exhibited ~11 times less activity than **3d**, but ~threefold more activity than **3a**. All the compounds showed lower activity than ascorbic acid (IC_{50} = 0.87 μM), a standard antioxidant agent.

Computational Studies. Phenolic Schiff bases have been reported to be strong antioxidants and powerful free-radical scavengers.[32,33] Because the antioxidant mechanism of phenolic antioxidants has been well established, it would be interesting to examine relationships between the electronic properties and molecular structures of nonphenolic hydrazone Schiff base antioxidants. To explain the DPPH free-radical scavenging mechanism of hydrazone Sciff base analogs **3a–e**, DFT calculations were carried out at the B3LYP/6-311G level to determine the electron densities, energies, FMO maps, and Mulliken charge distributions of the atoms composing the synthesized compounds.

The Mulliken charge distributions of all atoms in **3a–e** (Table 4) showed that the following atoms and bonds are bearing the higher values of negative charge: N9 (−0.570) and O17 (−0.403) for **3a**, N9 (−0.562), O17 (−0.402), —O18—C21— (−0.535, −0.292), and —O20—C19— (−0.538, −0.294) for **3b**, N9 (−0.570), and O17 (−0.398) for **3c**, N9 (−0.571), O17 (−0.411) and —C19—N18—C20— (−0.355, −0.664, −0.354) for **3d**, and N9 (−0.563), O17 (−0.396), and O19 (−0.369) for **3e**. This result indicates that these atom groups may be subjected to oxidation or loss of hydrogen attached to the N, O, or C atoms. Additionally, C2 (−0.261) attached to the chlorine atom in **3c**, C1 (−0.198) and C3 (−0.206) in **3d**, and C3 (−0.208) in **3e** also bear moderate negative charge,

Table 4. Mulliken charges (*e*) for compounds **3a–e**.

3a		**3b**		**3c**		**3d**		**3e**	
Atom	Charge/*e*	Atom	Charge/*e*	Atom	Charge/*e*	Atom	Charge/*e*	Atom	Charge/*e*
C(1)	–0.172	C(1)	–0.164	C(1)	–0.072	C(1)	–0.198	C(1)	–0.131
C(2)	–0.119	C(2)	0.264	C(2)	–0.261	C(2)	0.376	C(2)	–0.118
C(3)	–0.171	C(3)	0.214	C(3)	–0.073	C(3)	–0.206	C(3)	–0.208
C(4)	–0.141	C(4)	–0.157	C(4)	–0.145	C(4)	–0.152	C(4)	–0.102
C(5)	–0.0772	C(5)	–0.044	C(5)	–0.064	C(5)	–0.057	C(5)	–0.022
C(6)	–0.0731	C(6)	–0.056	C(6)	–0.075	C(6)	–0.090	C(6)	–0.111
C(7)	–0.008	C(7)	–0.013	C(7)	–0.001	C(7)	0.001	C(7)	0.024
N(8)	–0.132	N(8)	–0.136	N(8)	–0.141	N(8)	–0.158	N(8)	–0.148
N(9)	–0.570	N(9)	–0.562	N(9)	–0.570	N(9)	–0.571	N(9)	–0.563
C(10)	0.490	C(10)	0.486	C(10)	0.500	C(10)	0.498	C(10)	0.494
C(11)	–0.121	C(11)	–0.123	C(11)	–0.123	C(11)	–0.123	C(11)	–0.121
C(12)	–0.107	C(12)	–0.106	C(12)	–0.106	C(12)	–0.109	C(12)	–0.107
C(13)	–0.162	C(13)	–0.162	C(13)	–0.162	C(13)	–0.164	C(13)	–0.162
C(14)	–0.118	C(14)	–0.118	C(14)	–0.116	C(14)	–0.119	C(14)	–0.118
C(15)	–0.190	C(15)	–0.191	C(15)	–0.191	C(15)	–0.191	C(15)	–0.190
C(16)	–0.021	C(16)	–0.018	C(16)	–0.023	C(16)	–0.024	C(16)	–0.022
O(17)	–0.403	O(17)	–0.402	O(17)	–0.398	O(17)	–0.411	O(17)	–0.396
H(18)	0.155	O(18)	–0.535	Cl(18)	–0.007	N(18)	–0.664	C(18)	0.177
H(19)	0.156	C(19)	–0.294	H(19)	0.186	C(19)	–0.355	O(19)	–0.369
H(20)	0.154	O(20)	–0.538	H(20)	0.184	C(20)	–0.354	H(20)	0.164
H(21)	0.159	C(21)	–0.292	H(21)	0.167	H(21)	0.170	H(21)	0.162
H(22)	0.184	H(22)	0.165	H(22)	0.191	H(22)	0.168	H(22)	0.170
H(23)	0.148	H(23)	0.166	H(23)	0.152	H(23)	0.148	H(23)	0.190
H(24)	0.314	H(24)	0.185	H(24)	0.317	H(24)	0.175	H(24)	0.212
H(25)	0.183	H(25)	0.149	H(25)	0.185	H(25)	0.141	H(25)	0.323
H(26)	0.155	H(26)	0.312	H(26)	0.157	H(26)	0.312	H(26)	0.185
H(27)	0.154	H(27)	0.184	H(27)	0.157	H(27)	0.181	H(27)	0.156
H(28)	0.152	H(28)	0.155	H(28)	0.154	H(28)	0.152	H(28)	0.155
H(29)	0.180	H(29)	0.154	H(29)	0.180	H(29)	0.152	H(29)	0.153
		H(30)	0.152			H(30)	0.149	H(30)	0.180
		H(31)	0.179			H(31)	0.182	H(31)	0.144
		H(32)	0.191			H(32)	0.195		
		H(33)	0.206			H(33)	0.178		
		H(34)	0.175			H(34)	0.196		
		H(35)	0.192			H(35)	0.197		
		H(36)	0.202			H(36)	0.178		
		H(37)	0.175			H(37)	0.197		

Table 5. DPPH radical scavenging activity of compounds **3a–e**.

Compound	IC_{50} (μM)
3a	360
3b	164
3c	264
3d	11
3e	114
Ascorbic acid	0.87

and thus, could undergo oxidation. The N9 (–0.570) atom of **3a**, which bears a high electron density, and is attached to a hydrogen atom could generate a proton free radical to neutralize DPPH radicals, as shown in Figure 6 (Path I). Because hydrazone Schiff bases usually show keto-enol tautomerism[34] in solution and the O17 (–0.403) atom of **3a** bears high electron density, **3a** could also exert antioxidant activity via the mechanism shown in Figure 6 (Path II). In compound **3b**, the carbons of the two methoxyl groups, C19 (–0.294) and C21 (–0. 292), bear high electron density, and thus, could produce proton free radicals to neutralize DPPH. So, **3b** could exert its antioxidant activity according to the mechanism

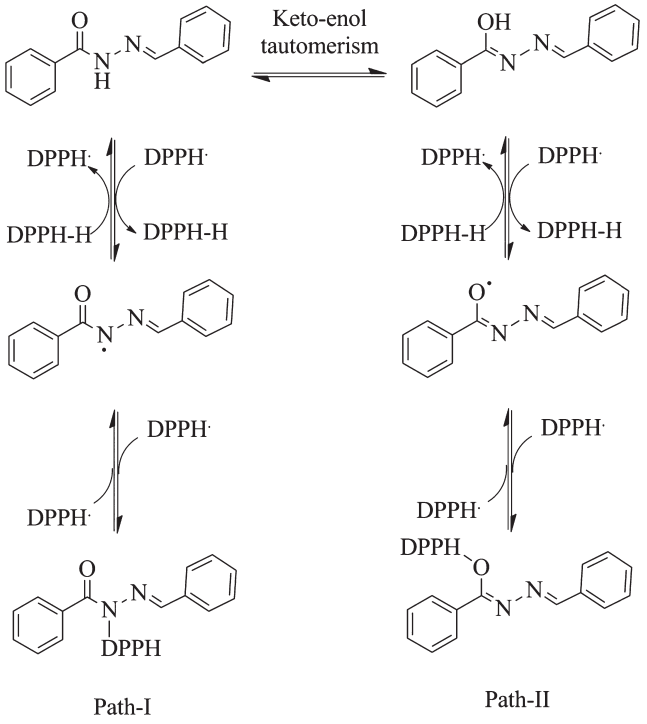

Figure 6. The proposed DPPH radical scavenging mechanism of (*E*)-*N*′-benzylidenebenzohydrazide (**3a**).

shown in Figures 6 and 7. Therefore, the antioxidant activity of **3b** is predicted to be higher than that of **3a**, which is consistent with our experimental data. In compound **3c**, C2 (−0.261), which is connected with the chlorine atom (−0.007) bears high negative charge, and thus, in addition to the mechanism shown in Figure 6, compound **3c** might also neutralize DPPH radicals via homolysis of the C2—Cl18 bond as the chlorine is more electronegative than the carbon. However, compound **3d** might exert its antioxidant activity via the formation of proton radicals attached to C19 (−0.355) and C20 (−0.354) (Figure 8) and via the mechanism shown in Figure 6. Whereas, O19 (−0.369) and C3 (−0.208) in compound **3e** bear high negative charge, which might enable protons attached to C18 and C2 to form proton radicals and scavenge DPPH.

Maps of the FMOs and of the energies of compounds **3a–e** are shown in Figure 5. The energy differences between HOMO and LUMO for **3a–e** were 6.19, 5.32, 5.218, 3.808, and 4.323 eV, respectively. Due to the lower energy difference between HOMO and LUMO for compound **3d**, the benzylidenebenzohydrazide radical would be more stable through resonance after the generation of proton free radicals than the corresponding radicals of **3a–c** and **3e**. However, the correlation coefficient (r^2) between HOMO–LUMO energy differences and the antioxidant activities of compounds **3a–e** was found to be 0.90

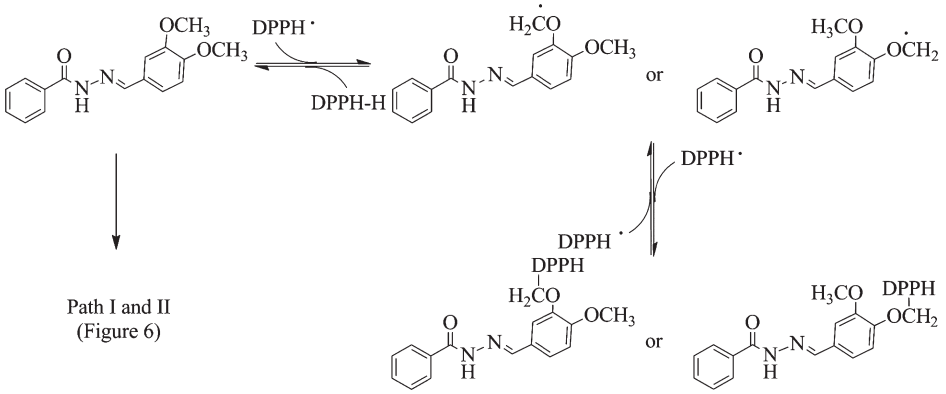

Figure 7. The proposed DPPH radical scavenging mechanism of (*E*)-*N*′-(3,4-dimethoxybenzylidene)benzohydrazide (**3b**).

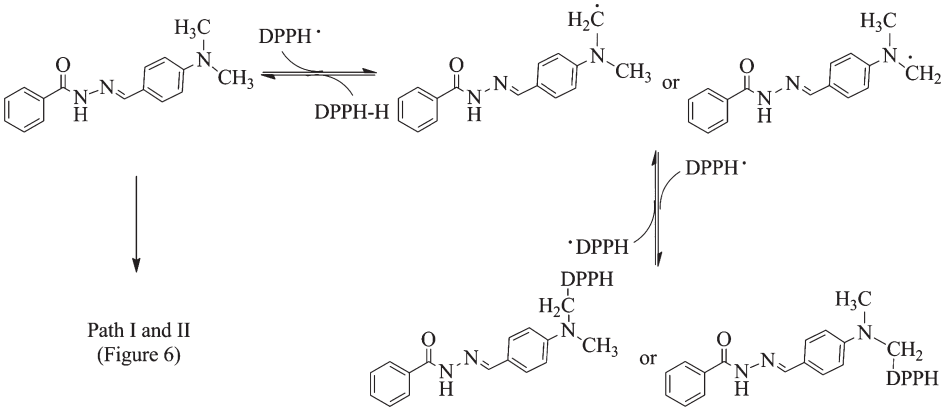

Figure 8. The proposed DPPH radical scavenging mechanism of (*E*)-*N*′-(4-(dimethylamino)benzylidene)benzohydrazide (**3d**).

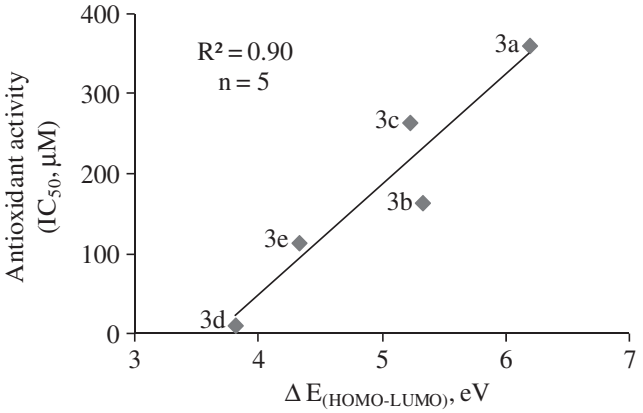

Figure 9. Correlation between antioxidant activity (IC_{50}, mM) and HOMO/LUMO energy differences of compounds **3a–e**.

($n = 5$), *i.e.*, antioxidant activity increased on decreasing HOMO and LUMO energy differences (Figure 9).

Conclusion

Nonphenolic (*E*)-*N*′-benzylidenebenzohydrazide analogs were synthesized and their antioxidant activity was evaluated using DPPH. A single crystal of (*E*)-*N*′-(4-chlorobenzylidene) benzohydrazide (**3c**) was obtained using the solvent loss technique and X-ray diffraction analysis revealed that it had triclinic symmetry (P-1) and a *trans* configuration around the azomethine (─C2═N2─) double bond. Weak nonclassical intermolecular N─H···O hydrogen bonds were observed on crystal layers and the crystal unit cell showed adjacent juxapositioned crystal layers. Hirshfeld analyses reveal the close O···H, N···H, Cl···H, and C···H contacts and π–π stacking in the crystal structure. All compounds showed significant DPPH radical scavenging activity, and of these, compound **3d** showed greatest activity with an IC_{50} value of 11 μM, although this was lower than that of the standard antioxidant, ascorbic acid ($IC_{50,}$ 0.87 μM). DFT studies revealed that protons attached to N, O, and C atoms with high negative charge might produce proton free radicals to neutralize DPPH. The study also indicates that low energy differences between HOMO and LUMO help to stabilize benzylidenebenzohydrazide radicals and increase activity. A good correlation was observed between HOMO–LUMO energy differences and the antioxidant activities of compounds **3a–e**.

Acknowledgments. Dr. Ha-Jin Lee at Korea Basic Science Institute (Western Seoul Center) is acknowledged for the X-ray analyses. Publication cost of this paper was supported by the Korean Chemical Society.

Supplementary Information. Crystallographic data for compound **3c** have been deposited at the Cambridge Crystallographic Data Center (Deposition number CCDC-1017656). Data can be obtained, free of charge, from: the Cambridge Crystallographic Data Center (CCDC), 12 Union Road, Cambridge, CB2 1EZ, UK; fax: +44(0) 1222–336033; e-mail: deposit@ccdc.cam.ac.uk; www.ccdc.cam.ac.uk/Community/Requestastructure/Pages/DataRequest.aspx

References

1. O. O. Ajani, C. A. Obafemi, O. C. Nwinyi, D. A. Akinpelu, *Bioorg. Med. Chem.* **2010**, *18*, 214.
2. L. Liu, M. S. Alam, Lee, D-U. *Bull. Korean Chem. Soc.* **2012**, *33*, 3361.
3. L. Savini, L. Chiasserini, V. Travagli, C. Pellerano, E. Novellino, S. Consentino, M. B. Pisano, *Eur. J. Med. Chem.* **2004**, *39*, 113.
4. Y. Janin, *Bioorg. Med. Chem.* **2007**, *15*, 2479.
5. J. R. Dimmock, S. C. Vasishtha, J. P. Stables, *Eur. J. Med. Chem.* **2000**, *35*, 241.
6. R. Kalsi, M. Shrimali, T. N. Bhalla, J. P. Barthwal, *Indian J. Pharm. Sci.* **2006**, *41*, 353.
7. C. Loncle, J. M. Brunel, N. Vidal, M. Dherbomez, Y. Letourneux, *Eur. J. Med. Chem.* **2004**, *39*, 1067.
8. M. T. Abdel-Aal, W. A. El-sayed, E. H. El-ashry, *Arch. Pharm. Chem. Life Sci.* **2006**, *339*, 656.
9. S.-J. Peng, *J. Chem. Crystallogr.* **2011**, *41*, 280.
10. A. El-Faham, M. Farooq, S. N. Khattab, A. M. Elkayal, M. F. Ibrahim, N. Abutaha, M. A. Wadaan, E. A. Hamed, *Chem. Pharm. Bull.* **2014**, *62*, 591.
11. C. D. Fan, H. Su, J. Zhao, B. X. Zhao, S. L. Zhang, J. Y. Miao, *Eur. J. Med. Chem.* **2010**, *45*, 1438.
12. H. H. Monfared, M. Nazari, P. Mayer, M.-A. Kamyabi, A. Erxleben, Z. Asgari, *Z. Naturforsch.* **2009**, *64b*, 409.
13. C. Juliano, A. Mattana, C. Solinas, *Transit. Met. Chem.* **2010**, *35*, 253.
14. O. Hashizume, A. Shimizu, M. Yokota, A. Sugiyama, K. Nakada, H. Miyoshi, M. Itami, M. Ohira, H. Nagase, K. Takenaga, *Proc. Natl. Acad. Sci. U.S A.* **2012**, *109*, 10528.
15. S. Bhattacharjee, L. J. Deterding, S. Chatterjee, J. Jiang, M. Ehrenshaft, O. Lardinois, D. C. Ramirez, K. B. Tomer, R. P. Mason, *Free Radic. Biol. Med.* **2011**, *50*, 1536.
16. C. Aliaga, E. A. Lissi, *Int. J. Chem. Kinet.* **1998**, *30*, 565.
17. E. Anouar, C. Calliste, P. Kosinova, F. di Meo, J. Duroux, Y. Champavier, K. Marakchi, P. Trouillas, *J. Phys. Chem. A* **2009**, *113*, 13881.
18. C. Iuga, J. R. Alvarez-Idaboy, A. Vivier-Bunge, *J. Phys. Chem. B* **2011**, *115*, 12234.
19. T. X. Nguyen, G. Grampp, A. V. Yurkovskaya, N. Lukzen, *J. Phys. Chem. A* **2013**, *33*, 7655.
20. A. López-Munguía, Y. Hernandez-Romero, J. Pedraza-Chaverri, A. Miranda-Molina, I. Regla, A. Martinez, E. Castillo, *PLoS One* **2011**, *6*, e201215.
21. Bruker, *SMART (Version 5.625) for Windows NT*, Bruker AXS Inc., Madison, WI, **2000**.
22. G. M. Sheldrick, *SHELXTL, Version 6.12 for Windows NT*, Bruker AXS Inc., Madison, WI, **2008**.
23. Bruker, *SAINT-Plus (Version 5.625) for Windows NT*, Bruker AXS Inc., Madison, WI, **2000**.
24. M. S. Blois, *Nature* **1958**, *181*, 1199.
25. M. J. S. Dewar, E. G. Zoebisch, E. F. Healy, *J. Am. Chem. Soc.* **1985**, *107*, 3902.
26. A. D. Becke, *J. Chem. Phys.* **1993**, *98*, 5648.
27. C. Lee, W. Yang, R. G. Parr, *Phys. Rev. B* **1988**, *37*, 785.

28. S. K. Wolff, D. J. Grimwood, J. J. McKinnon, M. J. Turner, D. Jayatilaka, M. A. Spackman, *Crystal Explorer (Version 3.1)*, University of Western Australia, Crawley, WA, **2012**.
29. M. Irfan, A. *Pharm. Sin.* **2011**, *2*, 102.
30. M. A. Spackman, D. Jayatilaka, *CrystEngComm* **2009**, *11*, 19.
31. F. H. Allen, O. Kennard, D. G. Watson, L. Brammer, A. G. Orpen, R. Taylor, *J. Chem. Soc., Perkin Trans. II* **1987**, *2*, S1.
32. E. H. Anouar, *Antioxidants* **2014**, *3*, 309.
33. A. N. Aziz, M. Taha, N. H. Ismail, E. H. Anouar, S. Yousuf, W. Jamil, K. Awang, N. Ahmat, K. M. Khan, S. M. Kashif, *Molecules* **2014**, *19*, 8414.
34. M. A. Kamyabi, S. Shahabi, H. Hosseini-Monfared, *J. Chem. Eng. Data* **2008**, *53*, 2341.

